C_{2v}[1,4,2] is reversed between $n = 3$ and $n = 4$. The bond lengths are all about 1.58 Å, and the particles lie close to the sphere that they are constrained to be on in the statics calculations. If the value of Q is increased from 1.228 to 12.28, then the bond lengths are longer (about 1.7 Å) and the D_{5h} structure is again the lowest energy geometry. Thus, the dynamics results include the static.

Field II. The equilibrium geometry is now C_1 (5040 isomers) with seven saddle-point geometries (the six from above plus the equilibrium geometry from above). The equilibrium geometry is shown in Figure 3, and some of the saddle-point geometries are shown in Figure 2. The energies associated with all geometries are shown in Table II. Clearly, field II creates a fluxional nightmare. Molecules for which field II gives an accurate representation of the repulsive potential would exhibit a ground-state dipole moment.[41]

Conclusions

Fields I and II provide insight into the preferred geometries of MX_n molecules. Field I is a more realistic field because it allows as many different bond lengths as there are local symmetries in a given MX_n structure. Field II on the other hand generates geometries that are independent of any bond length assigned to a MX_n structure and thus provides a standard for geometry in molecules where all pairs of the peripheral atoms try to be diametrically opposite one another. For MX_4 and MX_6 molecules, the energies of the equilibrium geometries are well below those of the nearest saddle-point ones, yet for MX_5 and MX_7 molecules, using the same force constants, there are saddle-point geometries that are easily accessible from the equilibrium geometry. These results agree with experimental results and imply that it is the repulsive interactions between the peripheral atoms and the intrinsic geometry of the molecules that determine their dynamic behavior. In addition, the details of the geometries are also in agreement with the results of quantum-mechanical calculations:[21,35] in MX_5, the axial bonds are longer than the equatorial ones, whereas in MX_7 they are shorter. The dynamical calculations can be made to imitate statics calculations by increasing the magnitude of the bond stretch force constant relative to the force constant Q. All isomers of a given geometry have the same potential energy with the result that derived statistical mechanical properties will have no bias.

In future work, we will use these simple potentials to study the details of isomer interconversion in MX_n molecules by scaling the force constants to give approximately correct vibrational frequencies and barrier heights.

Acknowledgment. H.-L.C. and J.F.G. acknowledge a grant from the South Carolina Energy Research and Development Center that enabled the purchase of the Digital MicroVax II computer.

(41) Kaiser, E. W.; Muenter, J. S.; Klemperer, W.; Falconer, W. E. *J. Chem. Phys.* **1970**, *53*, 53.

Contribution from the Fachbereich Chemie, Philipps-Universität, D-3550 Marburg, FRG, and Institute of General and Inorganic Chemistry, Bulgarian Academy of Sciences, 1040 Sofia, Bulgaria

Local and Cooperative Jahn-Teller Distortions of Ni^{2+} and Cu^{2+} in Tetrahedral Coordination

Dirk Reinen,*† Michail Atanasov,‡ Georgi St. Nikolov,‡ and Friedhelm Steffens†

Received July 8, 1987

A vibronic coupling model, including spin-orbit interactions, is presented and used to explain the sign and magnitude of observed Jahn-Teller distortions of Cu^{2+} and Ni^{2+} ions in tetrahedral coordination. It is demonstrated that the Jahn-Teller coupling is rather large for Cu^{2+} ($^2T_2$ ground state) and generally dominates over steric ligand, geometric packing, or spin-orbit effects, leading to compressed tetrahedra with D_{2d} symmetry. In contrast Ni^{2+} ($^3T_1$ ground state) undergoes much smaller Jahn-Teller interactions, and static distortions (elongated D_{2d} geometry) are not always expected. The lowering of the vibronic constants for Ni^{2+} as compared to Cu^{2+} is mainly due to the configuration interaction between the $^3T_1$ ground and excited states. The vibronic coupling analysis is based on spectroscopic and structural results of "CuO_4", "CuF_4", and "NiO_4" chromophores in various host structures. A quantitative discussion of the Jahn-Teller stabilization energies for the minima in the $T \otimes (e + t_2)$ adiabatic potential surface is given. The influence of elastic interactions between the tetrahedra (cooperative Jahn-Teller effect) on the ground-state splitting and on the extent of the local Jahn-Teller distortion is also considered. An essential energy contribution to the term splittings may arise from elastic interactions of this kind in structures with widely interconnected polyhedra.

Introduction

Cu^{2+} and Ni^{2+} ions in tetrahedral coordination have orbitally degenerate ground states $^2T_2$ and $^3T_1$, respectively and are expected to be subject to Jahn-Teller forces.[1] The induced symmetry lowering and term splittings due to the minima of the adiabatic Jahn-Teller (JT) surface can be detected by spectroscopic and structural studies. Whether a static or dynamic Jahn-Teller effect prevails depends on the depth of the various minima of the adiabatic potential surface (APS). While stable minima are known to arise only from second-order contributions for Cu^{2+} in octahedral coordination, in tetrahedral geometry such points are already produced by first-order terms. Static Jahn-Teller distortions have been observed in the case of $CuCl_4^{2-}$ entities and are interpreted within the angular overlap model (AOM).[2] Unlike Cu^{2+} the structural and spectral data on tetrahedral Ni^{2+} are scarce because this ion only reluctantly adopts this coordination.[3] The incorporation of Cu^{2+} and also Ni^{2+} into the tetrahedral sites of the spinel structure is possible, however, if the octahedral sites are blocked by Cr^{3+}.[3]

The aim of the present paper is to explain the sign and the magnitude of the static Jahn-Teller distortions in spinels with the constitution $[M_xZn_{1-x}]^t[Cr_2]^oO_4$ (M = Cu^{2+}, Ni^{2+}; o = octahedral; t = tetrahedral) on the basis of spectral and structural data. We will first present a vibronic coupling model—including spin-orbit coupling—which allows us to describe the Jahn-Teller distortions of tetrahedral Cu^{2+} and Ni^{2+} complexes. Then we will analyze spectral and structural data of MO_4 chromophores (M = Ni^{2+},

† Philipps-Universität.
‡ Bulgarian Academy of Sciences.

(1) Reinen, D. *Comments Inorg. Chem.* **1983**, *2*, 227.
(2) Bacci, M. *J. Phys. Chem. Solids* **1980**, *41*, 1267.
(3) Reinen, D.; Allmann, R.; Baum, G.; Jakob, B.; Kaschuba, U.; Massa, W.; Miller, G. J. *Z. Anorg. Allg. Chem.* **1987**, *548*, 7.

0020-1669/88/1327-1678$01.50/0

Cu^{2+}) in spinels and in square-planar arrangements and will subsequently report about spectra of tetrahedral and square-planar CuF_4^{2-} entities. In particular the following problem will be discussed: Why is the Jahn–Teller distortion considerably greater for Cu^{2+} than for Ni^{2+}? Finally, a full analysis of all possible minima in the adiabatic Jahn–Teller surface for the tetrahedral $^2T_2$ (d^9 configuration) and $^3T_1$ (d^8 configuration) ground states is given on the basis of the parameters derived for the Cu–O and Ni–O bonds.

Experimental Section

The preparation of the compounds was performed as described elsewhere.[3,4] The ligand field reflection spectra were recorded on a Zeiss PMQ II spectrophotometer (Infrasil) with a low-temperature attachment, by using Sr_2TeZnO_6 [(4–12) × 10^3 cm^{-1}] and freshly sintered MgO [(8–30) × 10^3 cm^{-1}] as standards. The data were converted into absorption values log (k/s), by following the theory of Schuster–Kubelka–Munk. The powder EPR spectra (35 GHz) were measured with a Varian E 15 spectrometer at 4.2, 77, and 298 K. DPPH was used as internal standard (g = 2.0037).

Jahn–Teller Distortions of Cu^{2+} and Ni^{2+} in Tetrahedral Coordination

A. Preliminary Remarks. The Jahn–Teller theorem, in particular its perturbational form due to Öpik and Price,[5] has provided a powerful tool for explaining and predicting molecular shapes as stationary points on a Born–Oppenheimer surface.[6] The theorem holds for degenerate electronic states in complexes of high symmetry and reveals which normal modes are able to destroy the initial symmetry. It cannot predict the ultimate symmetry of the distorted complex, however, if various distortion geometries are possible. In a recent study, Ceulemans et al.[7] examined in general terms the topology of an adiabatic T ⊗ (e + t_2) Jahn–Teller surface and used this particular case to formulate the epikernel principle, which states that the symmetry of the stable minima in an adiabatic Jahn–Teller surface is the highest possible one with lifted degeneracy: extremum points (minima, maxima, or saddle points) prefer epikernels to kernels and maximal epikernels to lower ranking epikernels. In fact this consideration is equivalent to Liehr's minimax principle[6] in group-theoretical terms. If we consider a T ground state of a tetrahedron, such as $^2T_2$ for the d^9 or $^3T_1$ for the d^8 configuration, the Jahn–Teller active vibrations are the bending e (Q_θ, Q_ϵ) and t_2 (Q_ξ, Q_η, Q_ζ) modes and the stretching t_2 (Q_ξ', Q_η', Q_ζ') normal vibration. The maximal (epikernel) symmetries of the T ⊗ e and T ⊗ t_2 direct products are D_{2d} and C_{3v}, respectively. The extremal points, together with the corresponding energies can be expressed in terms of the harmonic force constants K_e, K_t^b and K_t^s—the superscripts b and s standing for bending and stretching modes, respectively—the linear Jahn–Teller interaction parameters V_e, V_t^b and V_t^s, and the quadratic coupling constants L_e, L_t^b, and L_t^s. The quadratic constants result from the non totally symmetric part of the e ⊗ e and t_2 ⊗ t_2 symmetrized direct products. Bacci was the first to propose the use of ligand field theory in its AOM version to parametrize the linear Jahn–Teller coupling in terms of σ- and π-bonding parameters.[8] This approach was extended to obtain also the second-order Jahn–Teller coupling constants.[7] The angular overlap model is particularly suitable for the calculation of vibronic constants for bending modes.

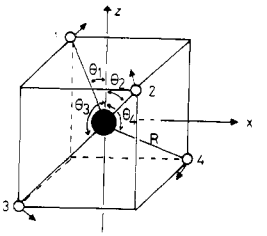

$$Q_\Theta = \frac{1}{2}R(-\Delta\Theta_1 - \Delta\Theta_2 + \Delta\Theta_3 + \Delta\Theta_4)$$

Figure 1. Geometry of a tetrahedron distorted along a S_4 axis [Q_θ(e) distortion path].

The first- and second-order vibronic constants for the T ⊗ (t_2 + e) problem—quadratic terms only for the bending modes, without those due to mixing between e and t_2 vibrations—obtained previously[7] are

$$V_e = \pm\frac{4(2^{1/2})}{3R}\left(e_\sigma - \frac{1}{3}e_\pi\right) \quad (1.1)$$

$$V_t^b = \pm\frac{2(2^{1/2})}{3R}\left(e_\sigma - \frac{7}{3}e_\pi\right) \quad (1.2)$$

$$V_t^s = \pm\frac{2}{3}\left(\frac{de_\sigma}{dR} - \frac{1}{3}\frac{de_\pi}{dR}\right) \quad (1.3)$$

$$L_e = \pm\frac{2}{R^2}\left(e_\sigma - \frac{5}{3}e_\pi\right) = L_t^b \quad (1.4)$$

The upper sign refers to a $^3T_1$ (d^8) and the lower sign to a $^2T_2$ (d^9) ground state. The experimental results on spinel mixed crystals and various other pseudotetrahedral $Cu^{II}L_4$ polyhedra, discussed below, will demonstrate that the vibronic coupling with the e mode is clearly dominant. This observation directly correlates with the AOM coupling constants, from which a V_e/V_t^b ratio larger than or equal (e_π = 0) to 2 (eq 1.1 and 1.2) is derived. Though V_t^s is even somewhat greater than V_e, the energetic effect induced by the t_2 stretching mode is expected to be much smaller, because the force constant K_t^s is considerably larger than K_e (vide infra). We will hence restrict ourselves to the T ⊗ e problem, which is elaborated in the Appendix and which leads to D_{2d} deformations of the parent T_d symmetry (epikernel principle for the T ⊗ e interaction). $Q_\theta > 0$ and $Q_\theta < 0$ are defined as due to tetragonal elongations and compressions, respectively (Figure 1). While the $Q_\theta = \rho\cos\phi$ and $Q_\epsilon = \rho\sin\phi$ components of the e mode transform the tetrahedral entity into D_{2d} symmetry for ϕ = 0°, 120°, and 240° or 180°, 300°, and 60°, any angular parameter deviating from these angles induces the lower D_2 symmetry in the ground-state potential surface. The displacements along Q_θ [φ = 0°(180°)] are given by

$$\overset{+}{(-)}\rho = \frac{1}{2}R(-\Delta\theta_1 - \Delta\theta_2 + \Delta\theta_3 + \Delta\theta_4) = R[(2\theta)_t - 2\theta] \quad (2)$$

where the angles $\Delta\theta_i$ are defined in Figure 1 and $(2\theta)_t$ and 2θ are the tetrahedral angle 109.47° and the corresponding angle in D_{2d} symmetry, respectively.

B. Ground-State Splittings in D_{2d}. The cross section of the adiabatic potential surface along the D_{2d} distortion pathway yields the following state energies for Cu^{2+} (T_2 ground state, compression):

$$E[{}_a\Gamma_6] = \frac{1}{2}K_e\rho^2 + \frac{1}{2}|V_e|\rho - \frac{1}{2}\zeta$$

$$E[{}_{a,b}\Gamma_7] = \frac{1}{2}K_e\rho^2 + \frac{1}{4}\left[-|V_e|\rho + \zeta \pm 3\left(V_e^2\rho^2 + \zeta^2 + \frac{2}{3}\zeta|V_e|\rho\right)^{1/2}\right] \quad (3)$$

For Ni^{2+} (T_1 ground state, elongation) the following state energies are obtained:

(4) Reinen, D.; Grefer, J. *Z. Naturforsch., B: Anorg. Chem. Org. Chem.* **1973**, *28a*, 1185.
(5) Öpik, U.; Pryce, M. H. L. *Proc. R. Soc. London, A.* **1957**, *238*, 425.
(6) Liehr, A. D. *J. Chem. Phys.* **1963**, *67*, 389.
(7) Ceulemans, A.; Beyens, D.; Vanquickenborne, L. G. *J. Am. Chem. Soc.* **1984**, *106*, 5824.
(8) (a) Bacci, M. *Chem. Phys. Lett.* **1978**, *58*, 537. (b) Bacci, M. *Chem. Phys.* **1979**, *40*, 237.

$$E[\Gamma_3] = E[\Gamma_4] = \frac{1}{2}K_e\rho^2 + \frac{1}{2}|V_e|\rho - \frac{1}{2}\zeta$$

$$E[\Gamma_2] = \frac{1}{2}K_e\rho^2 + \frac{1}{2}|V_e|\rho + \frac{1}{2}\zeta$$

$$E[_{a,b}\Gamma_5] = \frac{1}{2}K_e\rho^2 + \frac{1}{4}\left[-|V_e|\rho \pm 3\left(V_e^2\rho^2 + \frac{4}{9}\zeta^2\right)^{1/2}\right]$$

$$E[_{a,b}\Gamma_1] = \frac{1}{2}K_e\rho^2 + \frac{1}{4}\left[-|V_e|\rho + \zeta \pm 3\left(V_e^2\rho^2 + \zeta^2 + \frac{2}{3}|V_e|\zeta\rho\right)^{1/2}\right] \quad (4)$$

Spin–orbit coupling was explicitly included [free ion values for the LS-coupling parameters: $\zeta_0(Cu^{2+}) = -830$ cm^{-1}; $\zeta_0(Ni^{2+}) = -625$ cm^{-1}]. The energies of the three Kramers' doublets of tetrahedral Cu^{2+} result from the solution of the $T_2 \otimes \Gamma_7 \otimes e(Q_\theta)$ vibronic problem, where Mulliken and Bethe notations are used for space and spin functions, respectively (see Figure 2). Similarly the energies of the seven states of tetrahedral Ni^{2+} originate from the $T_1 \otimes \Gamma_4 \otimes e(Q_\theta)$ coupling.

We shall now consider the mixing of excited electronic terms with the ground state. Such mixing is not present in case of copper(II) but may be important for tetrahedral Ni(II) complexes. If configuration interaction of the electronic $^3T_1$ ground state in T_d with the excited state of the same symmetry (see Figure 6, T_d) is taken into account, the vibronic coupling parameters V_e and L_e and the LS coupling constant ζ for the ground state should be regarded as effective values and have to be replaced as follows:

$$V_e^{eff} \equiv (a^2 - b^2)V_e - b^2V_e'$$

$$L_e^{eff} \equiv (a^2 - b^2)L_e + b^2L_e'$$

$$\zeta^{eff} \equiv \left(a^2 - \frac{1}{2}b^2 + 2ab\right)\zeta \quad (5)$$

These expressions were derived by using an operator-equivalent technique. The constants a and b (both >0) are the term mixing coefficients in the ground-state wave function, which depend on the cubic field splitting parameter Δ_t and the Racah parameter B:

$$\psi_g = a\psi[^3_aT_1] - b\psi[^3_bT_1] \quad (6)$$

The vibronic coupling constants V_e' and L_e' (see definitions in Appendix) are calculated in the AOM as

$$V_e' = \frac{4(2^{1/2})}{3R}e_\pi \quad (1.5)$$

$$L_e' = \frac{2}{3R^2}e_\pi \quad (1.6)$$

It can readily be seen from eq 5 that the configuration interaction reduces the linear vibronic constant, while ζ^{eff} and ζ differ only slightly. The second-order vibronic constant L_e is also reduced, but to a smaller extent. The Hamiltonian and the energy matrices, which yield eq 3 and 4, are given in the Appendix.

We will now briefly discuss the ground-state energies in terms of the vibronic coupling constants. Figures 2 and 7a show cross sections of the potential energy surfaces for the split-term manifolds of $^3T_1$ and $^2T_2$ along the Q_θ distortion coordinate. The parameter values were chosen according to the spectra analyses of Cu^{2+} and Ni^{2+} doped into the $ZnCr_2O_4$ spinel (vide infra). Without discussing the chosen parameters at present, it is clearly seen, that Cu^{2+}—in contrast to Ni^{2+}—undergoes a significant Jahn–Teller distortion.

If quadratic Jahn–Teller coupling terms are taken additionally into account, the full matrices as given in the Appensix should be used. For vanishing spin–orbit coupling, the D_{2d} extremal points

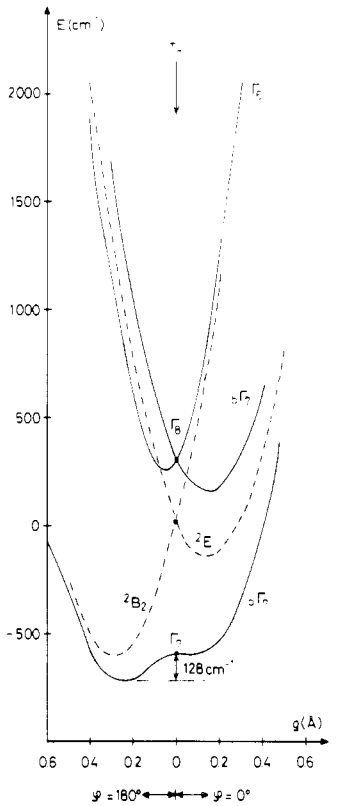

Figure 2. Cross section of the potential energy surface along the Q_θ normal coordinates (φ = 0 and 180°, 120 and 300°, or 240 and 60°), arising from the $^3T_2$ ground state of tetrahedral Cu^{2+}. Solid and dashed curves, denote cross sections with and without LS coupling, respectively. Parameters: e_σ = 4900 cm^{-1}, e_π = 1400 cm^{-1}, e_{sd} = 1800 cm^{-1}, ζ = −600 cm^{-1}, and K_e^* = 15 100 cm^{-1}/Å^2.

on the $^3A_2$ (Ni^{2+}) and $^2B_2$ (Cu^{2+}) potential sheets are characterized by

$$\rho_m = \frac{|V_e|}{K_e + L_e}$$

$$E_m = -\frac{1}{2}\frac{V_e^2}{K_e + L_e} = -\frac{1}{2}\rho_m|V_e| \quad (7)$$

(in eq 7 and 8 V_e and L_e should be replaced by V_e^{eff} and L_e^{eff} for Ni^{2+}) where the quadratic vibronic constants L_e (eq 1.4) have different signs for Cu^{2+} and Ni^{2+}. Apparently, the higher order terms reduce the extent of distortion in the case of Ni^{2+}, while larger ligand displacements are expected for Cu^{2+} tetrahedra. The splitting of the parent $^3T_1$ or $^2T_2$ states at ρ_m is given by

$$E(E) - E(A_2 \text{ or } B_2) = \frac{3}{2}\rho_m|V_e|\frac{K_e + \frac{1}{2}L_e}{K_e + L_e} \quad (8)$$

Results

For spinel phases $Zn_{1-x}M_xCr_2O_4$ with a normal cation distribution, transitions to tetragonal structures with $c/a < 1$ and $c/a > 1$ for M = Cu^{2+} and Ni^{2+}, respectively, are observed with increasing x. They are induced by ferrodistortive elastic interactions between the distorted compressed Cu^{2+} or elongated Ni^{2+} tetrahedra.[3,4] The compressed copper tetrahedra (spacings 1.94 Å)[9] show a significantly larger deviation from the tetrahedral angle 109.47°, namely $\Delta(2\theta) = +13°$,[9] than the elongated NiO_4 tetrahedra ($\Delta(2\theta) = -7°$ (spacings 1.93 Å).[10] Unlike Ni^{2+} and Cu^{2+} the isomorphous substitution of Co(II) into the $ZnCr_2O_4$ spinel produces no phase transition; the site symmetry remains T_d ($^4A_2$ ground state). While the mentioned spinel mixed crystals are cubic at low concentrations of Cu^{2+} and Ni^{2+}, the transitions to the tetragonal phases are observed at the critical concentrations (298

(9) Prince, E. *Acta Crystallogr.* **1957**, *10*, 554.
(10) Prince, E. *J. Appl. Phys.* **1961**, *32*, 68 S.

Table I. Vibronic Coupling, Elastic and AOM Parameters for Mixed Crystals $Zn_{1-x}M_xCr_2O_4$ (M = Cu^{2+}, Ni^{2+})

	V_e, cm^{-1}/Å	S_e, cm^{-1}/Å	e_σ, cm^{-1}	e_π, cm^{-1}	e_{sd}, cm^{-1}	L_e, cm^{-1}/Å	K_e, cm^{-1}/Å^2
Cu^{2+}	−4300	−2500	4900	1400	1800	−1350	16450
Ni^{2+}	2900[a]	1550	4700	1300	500	1050[a]	*b*

[a] Effective values (eq 5), with configuration interaction accounted for. [b] For the NiO_4 tetrahedron about the same force constant is expected as the one calculated for CuO_4.

K), namely $x = 0.47$ for $Cu^{3,4}$ and $x = 0.97$ for Ni^3. The end members of the mixed crystal series transform to cubic structures at ≃900 K ($CuCr_2O_4$[11]) and 298 K ($NiCr_2O_4$[12]).

A. Cu^{2+} Tetrahedra in Spinel Phases. The electronic spectra of mixed crystals $Zn_{1-x}Cu_xCr_2O_4$ have been reported elsewhere.[4] For $x = 1$ two rather broad d–d bands are observed at 4500 and 8300 cm^{-1} (298 K), which correspond to the transitions $^2B_2 \rightarrow {}^2E$ (within the T_2 ground-state split terms) and $^2B_2 \rightarrow {}^2A_1$ in D_{2d}, respectively. The transition $^2B_2 \rightarrow {}^2B_1$ ($^2A_1$ and $^2B_1$ are split states of the tetrahedral ^2E parent level) is symmetry forbidden in D_{2d}. Both the ground-state splitting and the structural angle $2\theta = 122.5°$, reported for $CuCr_2O_4$, reflect the local Jahn–Teller distortion as well as the cooperative elastic forces, which are responsible for the phase transition from cubic to tetragonal. These forces can be formally treated analogous to the linear vibronic coupling and give rise to the strain parameter S_e[13] (see Appendix), which represents the molecular elastic field of neighboring Cu^{2+} tetrahedra at any Cu^{2+} center. Following the model proposed by Woitowicz[14] for the elastic interactions between Jahn–Teller active centers within the spinel structure, we have calculated $|S_e|\rho \simeq 1100$ cm^{-1} from the critical temperature $T_c \simeq 900$ K. S_e and V_e can now be derived from the distortion of the CuO_4 tetrahedra in $CuCr_2O_4$ ($\rho = 0.44$ Å; eq 2) and the observed ground-state splitting $\Delta E \simeq 3/2(|V_e|\rho + |S_e|\rho)$ (eq 8 with $L_e = 0$). The AO parameters e_σ and e_π, listed in Table I, are obtained from V_e (eq 1.1), assuming a reasonable value for the tetrahedral ligand field parameter $\Delta_t = {}^4/_9(3e_\sigma - 4e_\pi)$. We have chosen the value found for Co^{2+} doped into the tetrahedral site of $ZnAl_2O_4$ (≃4000 cm^{-1}), because Ni^{2+}, Co^{2+}, and Cu^{2+} produce very similar Δ parameters in equivalent compounds. The energy contributions to the term splittings induced by the elastic interactions between the distorted CuO_4 tetrahedra ("cooperative Jahn–Teller effect") are quite large, indicating a strong influence on the Cu–O bonding properties. We have deduced the AO parameters from only that part of the ground-state splitting, which is not due to the strain energy (≃$^3/_2|S_e|\rho$). A parametrization without correcting for the latter contribution would result in effective e_σ and e_π values, which are strongly dependent on the Cu^{2+} concentration in the mixed crystals $Zn_{1-x}Cu_xCr_2O_4$—in contrast to the average Cu–O bond length, which does not vary with x.[4] The derived AO parameters hence refer to CuO_4 tetrahedra, which are distorted by solely a local Jahn–Teller effect, and may be more easily transferred to other oxidic solids with Cu^{2+} ions than "effective" parameters, which additionally reflect varying contributions due to cooperative–elastic interactions. The local distortion, as expected for x values below the critical concentration $x_c = 0.47$ of the phase transition at 298 K, can be calculated by using the ratio

$$\frac{\rho_{local}}{\rho_{x=1}} = \frac{|V_e|}{|V_e| + |S_e|} \qquad (9)$$

It is derived from (7) on the assumption that second-order contributions to the cooperative elastic forces are only small and K_e does not change significantly at the phase transition. With $\rho_{x=1} = 0.44$ Å and V_e and S_e from Table I, a local radial distortion parameter of 0.28 Å results, corresponding to compressed tetrahedra with $2\theta \simeq 118°$. The term energies for the CuO_4 polyhedron are plotted versus ρ and 2θ in Figure 3. The e_σ and e_π parameters of Table I were used, supplemented by e_{ds} (vide infra), which was derived from the $^2B_2 \rightarrow {}^2A_1$ transition energy, and a spin–orbit coupling constant, which is reduced by covalency with respect to ζ_0 by about 27%. The ${}_a\Gamma_7(^2B_2) \rightarrow {}_b\Gamma_6(^2A_1)$ transition is predicted to occur at 6150 cm^{-1} for $\rho = 0.28$ Å ($x < 0.47$), which compares well with the experimental value of 6200 cm^{-1}.[4] The same transition is expected at 7150 cm^{-1} for $CuCr_2O_4$ ($\rho = 0.44$ Å, see Figure 3). To this "local" energy, $\rho_{x=1}|S_e| = 1100$ cm^{-1} has to be added, yielding ≃8250 cm^{-1}, which is again very near to the observed band energy of 8300 cm^{-1}.[4] The cooperative contribution is presumably quite large in case of the spinel lattice, because the polyhedra are widely interconnected in this structure type, leading to strong elastic interactions.

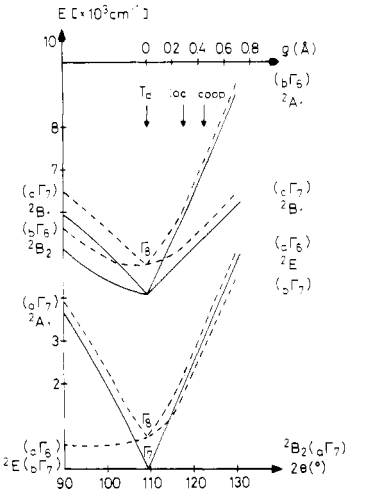

Figure 3. Term energies of CuL_4 polyhedra in T_d and D_{2d} symmetry versus the radial distortion parameter ρ or the tetrahedral angle 2θ. Parameters: $e_\sigma = 4900$ cm^{-1}, $e_\pi = 1400$ cm^{-1}, $e_{sd} = 1800$ cm^{-1}, and $\zeta = -600$ cm^{-1}. Solid and dashed curves denote energies without and with LS coupling; the arrows mark the characteristic ρ values of 0.28 and 0.44 Å (see text).

While Figure 3 gives only the electronic energies, Figure 2 comprises the results of the vibronic calculations. The chosen force constant K_e^* was derived from the known values of $|V_e|$ and ρ by following (7), but with the inclusion of LS coupling. K_e^* is an effective number and actually the sum of the true force constant K_e and the second-order vibronic coupling constant L_e, which is calculated from (1.4) as −1350 cm^{-1} Å^{-2} (−0.03 mdyn Å^{-1}) (Table I). From the calculated local force constant $K_e = 16450$ cm^{-1} Å^{-2} one obtains an energy of 325 cm^{-1} for the e bending mode of the CuO_4 tetrahedra in the spinel lattice. The value of K_e (0.32 mdyn Å^{-1}) is rather high compared to those for CuX_4^{2-} complexes (for X = Br^-, Cl^-, and F^- they are 0.10, 0.11, and 0.17 mdyn Å^{-1}, respectively; compare also Table II). We think that the rigidity of the e mode is enhanced, because the polyhedra are widely interconnected in the spinel structure, while the mentioned CuX_4^{2-} polyhedra are isolated in the respective lattices.

The cross section of the potential energy surface of the ground state of tetrahedral Cu^{2+} along the Q_θ normal coordinate demonstrates that the stabilization of the flattened tetrahedron relative to a slightly elongated tetrahedron is ≃125 cm^{-1} (Figure 2). If the LS-coupling constant is further reduced (for example by the Ham effect[15]) the stabilization energy increases considerably (≃450 cm^{-1} for $\zeta = 0$). By inspection of the cross section of the ground-state potential energy surface perpendicular to the energy axis (Figure 4), it is immediately evident that the system can move between the three equivalent D_{2d} minima at $\rho = 0.28$ Å and $\varphi = 180°$, 300°, and 60°, if the saddle-points at $\varphi = 0°$, 120°, and 240° are surpassed by thermal motion (dynamic Jahn–Teller effect). In the presence of cooperative elastic interactions, only one minimum at $\varphi = 180°$ remains ($\rho = 0.44$ Å, $E_{min} \simeq -1600$ cm^{-1}). Above the phase transitions of mixed crystals

(11) Ohnishi, H.; Teranishi, T. *J. Chem. Soc. Jpn.* **1961**, *16*, 35.
(12) Sawaoka, A.; Tomizuka, C. T. *J. Phys. Soc. Jpn.* **1974**, *36*, 912.
(13) Englman, R. *The Jahn–Teller Effect in Molecules and Crystals*; Wiley-Interscience: London, England, 1972.
(14) Woitowicz, P. J. *Phys. Rev.* **1959**, *116*, 32.
(15) Ham, F. S. *Phys. Rev. A* **1965**, *138*, 1727.

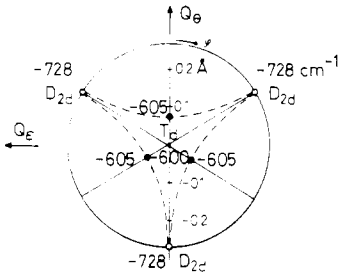

Figure 4. Cross section of the adiabatic potential energy surface of tetrahedral Cu^{2+} ($T_2 \otimes e$ problem) perpendicular to the E axis, without cooperativity (the energetically most favorable pathway between the minima is additionally marked). Parameters: see Figure 2.

$Cu_xZn_{1-x}Cr_2O_4$, the elastic constant S_e is nearly zero and only the local Jahn–Teller distortion remains. Because the energy barrier between the three minima is $\simeq$125 cm^{-1} (Figure 4)—or 610 cm^{-1} at most, when spin–orbit coupling is quenched completely by the Ham effect—the distortion is expected to be dynamic above a critical temperature of 200 K (900 K). Unfortunately the EPR spectra are disturbed by strong magnetic interactions between Cu^{2+} and Cr^{3+}, leading to exchange coupled signals, which are not indicative with respect to dynamic or static distortions of the CuO_4 polyhedra.[4]

We will report on the concentration dependence of the strain parameter S_e and the phase diagrams (x versus T_c) of mixed crystals $Zn_{1-x}M_xCr_2O_4$ [M = Cu^{2+}, Ni^{2+}] in a separate paper.

B. Cu^{2+} in Square-Planar Coordination. It seems promising to compare the results obtained for the flattened CuO_4 tetrahedra in the spinel structure with those for the square-planar CuO_4 coordination in Li_2CuO_2, because the latter may be regarded as the limiting geometry of tetragonally compressed tetrahedra. The CuO_4 entities are corner-connected and form layers in the Li_2MO_2 (M = Cu^{2+}, Ni^{2+}) structure. The bands at 14000 and 17000 cm^{-1} in the 5 K reflectance spectrum of Li_2CuO_2 with Cu–O spacings of $\simeq$1.97 Å[16] (Figure 5) are assigned to the transitions from $^2B_{2g}$ to $^2B_{1g}$ and ^2E_g, respectively, and the shoulder around 21000 cm^{-1} is due to the $^2B_{2g} \rightarrow {}^2B_{1g}$ transition,[17] yielding e_σ = 6800 cm^{-1}, e_π = 1600 cm^{-1}, and e_{ds} = 1800 cm^{-1}. The parameter e_{ds} describes interactions of the nd with the $(n+1)$s orbitals in D_{4h} symmetry.[18] The e_{ds} value derived for Li_2CuO_2 has also been used for the spinel mixed crystals, discussed above. The derived AO parameters should be considered as effective values, because no corrections with respect to cooperativity contributions have been made. The same argument holds for the AO parameters of Egyptian blue,[4] also with CuO_4 square planes [a(Cu–O) = 1.91 Å],[19] imbedded into an array of interconnected polyhedra: e_σ = 6500 cm^{-1}, e_π = 1800 cm^{-1}, and e_{ds} = 1400 cm^{-1}. They are very similar to those of Li_2CuO_2 and to those of $CuCr_2O_4$, if no corrections with respect to the cooperative elastic Jahn–Teller forces are made.

The EPR powder spectrum of Li_2CuO_2 is axial with g values $g_\parallel = 2.26_3$ and $g_\perp = 2.05_2$. They are indicative of a d_{xy} ground state,[17] as expected for CuO_4 square planes. From the orbital contributions a covalency parameter $k_\parallel \simeq k_\perp \simeq 0.75$ is calculated:

$$g_\parallel = g_0 + 8u_\parallel - 3u_\perp{}^2 - 4u_\parallel u_\perp$$

$$u_{\parallel(\perp)} = \frac{k_{\parallel(\perp)}{}^2|\zeta_0|}{E[B_{2g} \rightarrow B_{1g}(E_g)]} \qquad (10)$$

$$g_\perp = g_0 + 2u_\perp - 4u_\parallel{}^2$$

Square planar entities, which are isolated from each other, are found in the structure of $CaCuF_4$. Cooperative elastic interactions are hence expected to be small, in accord with the results discussed below. With the assignment $^2B_{2g} \rightarrow {}^2B_{1g}$, $^2A_{1g}$, and ^2E_g for the ligand field transitions at 10100, 13300, and 13800 cm^{-1} (Figure 5), we obtain e_σ = 5850 cm^{-1}, e_π = 1850 cm^{-1} ($\Delta = 3e_\sigma - 4e_\pi \simeq$ 10000 cm^{-1}), and e_{ds} = 400 cm^{-1}. The assignment is consistent with the EPR results. The molecular g values, which are calculated from the exchange-coupled g tensor of $CaCuF_4$,[20] are $g_\parallel = 2.46_2$ and $g_\perp = 2.07_5$. With (10), we derive the covalency parameter $k_\parallel \simeq k_\perp \simeq 0.85$, which is much larger than the one for Li_2CuO_2—as expected for the more electronegative F^- ligand. Very interesting results came from Cu^{2+} incorporated in the 4-coordinate Zn^{2+} sites of $CaZnF_4$,[21] one of the rare examples with a transition-metal ion in a tetrahedral environment of F^- ions. For $CaZn_{0.93}Cu_{0.07}F_4$ two rather intense transitions at 5200 and 8500 cm^{-1} are observed in the 5 K reflection spectrum, with an additional weak absorption around 6700 cm^{-1}. The three bands can be assigned to the $^2B_2 \rightarrow {}^2E$, $^2A_1$ and the symmetry forbidden $^2B_2 \rightarrow {}^2B_1$ transitions in D_{2d}, respectively. With the AO parameters from $CaCuF_4$ the observed band energies can be reproduced within 100 cm^{-1}, if $2\theta \simeq 129°$ is chosen. Though the ZnF_4 tetrahedra in the host lattice are already tetragonally compressed by packing forces ($2\theta \simeq 116.8°$),[21] 2θ has increased by about 12° for the CuF_4 polyhedra—clearly indicating a significant Jahn–Teller contribution to the overall distortion. The g tensor of the doped compound ($g_\parallel = 2.61_6$, $g_\perp = 2.20_8$) is in accord with the assignment of the ligand field spectrum. The interpretation on the basis of (10) yields covalency factors $k_\parallel \simeq k_\perp \simeq 0.85 \pm 0.01$, in excellent agreement with those of $CaCuF_4$. A continuous mixed-crystal series between the end members $CaZnF_4$ (Scheelite structure) and $CaCuF_4$ ($KBrF_4$ type structure) does not exist.

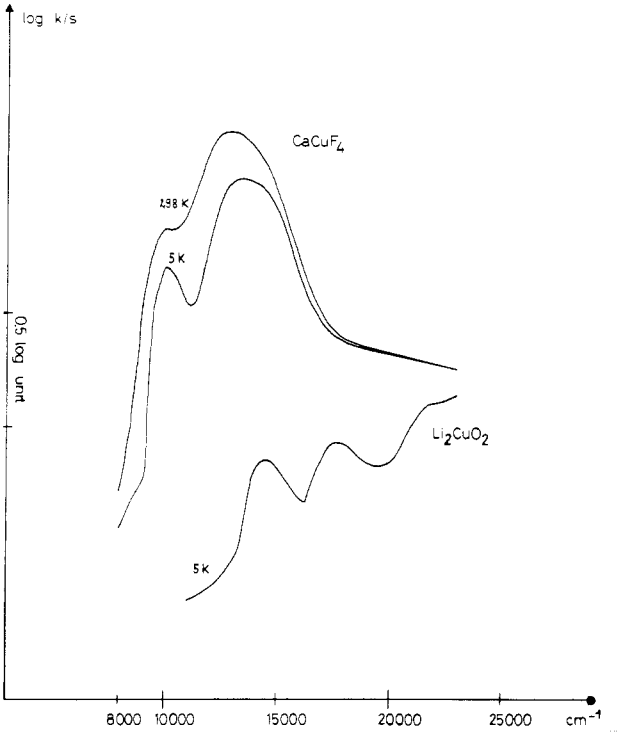

Figure 5. Electronic reflectance spectra of $CaCuF_4$ and Li_2CuO_2.

C. Ni^{2+} in Square-Planar Coordination. Li_2NiO_2 is isostructural with Li_2CuO_2 and represents a very interesting and rare example of a paramagnetic Ni(II) square-planar chromophore. The Ni–O spacings in the NiO_4 square planes are 1.90 Å.[22] Axial contacts to oxygen atoms of other NiO entities are very weak ($\simeq$3.7 Å). The reflection spectrum consists of three bands and two shoulders (Figure 6). Using the energy matrices for a d^8 cation in a

(16) Rieck, H.; Hoppe, R. *Z. Anorg. Allg. Chem.* **1971**, *379*, 159.
(17) In order to directly correlate the axes in the T_d and D_{2d} point groups with those in the square-planar coordination, the coordinate system of Figure 1 was also used for the orbital and term notations in the point group D_{4h} (nonstandard setting).
(18) Smith, D. W. *Inorg. Chim. Acta* **1977**, *22*, 107. Hitchman, M. A.; Bremner, J. B. *Inorg. Chim. Acta* **1978**, *27*, L61.
(19) Clark, M. G.; Burns, R. G. *J. Chem. Soc. A* **1967**, 1034.
(20) Reinen, D.; Dance, J.-M. *Inorganic Solid Fluorides*, Academic: London, 1985; p 525.
(21) von Schnering, H. G.; Bleckmann, P. *Naturwissenschaften* **1965**, 538.
(22) Rieck, H.; Hoppe, R. *Z. Anorg. Allg. Chem.* **1972**, *392*, 193.

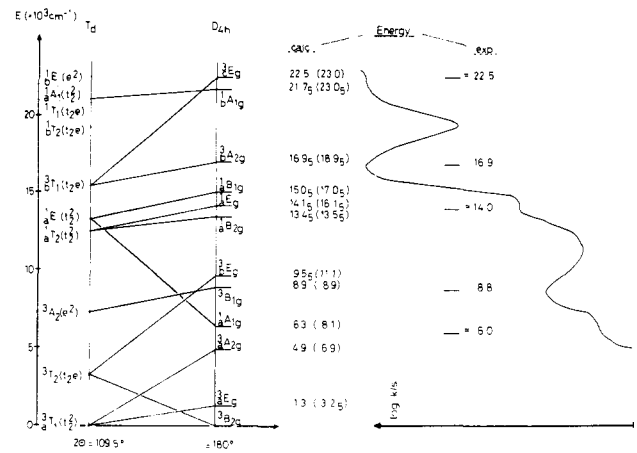

Figure 6. Electronic reflectance spectrum of Li_2NiO_2 at 5 K and band assignment in D_{4h} symmetry. Parameters (in 10^3 cm^{-1}): $e_\sigma = 4.7$, $e_\pi = 1.3$, $e_{sd} = 0.5(0.0)$, and $B = 0.85$; $C/B = 4.3$. The correlation of the terms in D_{4h} with those in T_d is also given.[17]

square-planar coordination, we have calculated the transition energies as a function of the AOM bonding parameters e_σ and e_π, taking into account nonzero e_{sd} values. We have explicitly checked the possibility of changing the ground-state multiplicity upon variations of e_σ, e_π, and e_{sd}. The values of the Racah parameters are $B = 850$ cm^{-1} and $C = 4.3B$, in line with previous results on Ni^{2+}–oxygen chromophores.[23]

The calculated d–d transition energies on the basis of the best fit parameters (in 10^3 cm^{-1}), $e_\sigma = 4.7 \pm 0.35$, $e_\pi = 1.3 \pm 0.45$, and $e_{sd} = 0.50 \pm 0.05$, are compared with the experimental values in Figure 6. The correlation with the parent T_d levels is also shown.[17] The electronic groundstate is $^3B_{2g}$ (z^2, xy), which originates from the first excited $^3T_{2g}$ state in T_d symmetry. The d–d transition energies are as follows (only diagonal terms):

$$^3B_{2g} \rightarrow {}^3_aE_g = 3B - 2e_\pi + e_\sigma - 4e_{sd}$$

$$^3_aA_{2g} = 3B - 4e_\pi + 4e_\sigma - 4e_{sd}$$

$$^3B_{1g} = 3e_\sigma - 4e_\pi$$

$$^3_bE_g = 4e_\sigma - 6e_\pi - 4e_{sd}$$

$$^3_bA_{2g} = 12B + e_\sigma - 4e_\pi - 4e_{sd}$$

$$^3_cE_g = 12B + 3e_\sigma - 2e_\pi$$

The transitions to $^3B_{1g}$ and $^3_cE_g$ are (nearly) independent of s–d interactions, while all others are lowered in energy by $\simeq 4e_{sd}$. The spectral assignment in Figure 6 is only quantitatively satisfactory, if a small, but nonvanishing e_{ds} value is assumed. Low intensities are expected for the two electron jumps $^3B_{2g} \rightarrow {}^3_aA_{2g}$ and $^3_bE_g$; this is not in contradiction to the observation. The shoulder at $\simeq 14000$ cm^{-1} seems to be due to a series of triplet–singlet transitions.

Though—in analogy to Li_2CuO_2—rather large effective AO parameters are expected, the obtained e_σ and e_π values are comparatively small and seem to reflect a rather anomalous bonding situation (see below). The energy of the $^3B_{2g} \rightarrow {}^3B_{1g}$ transition is just the cubic ligand field splitting, $3e_\sigma - 4e_\pi$ (8900 cm^{-1}). It is very low compared to the value of 14 000 cm^{-1} for Li_2CuO_2 (section B) and resembles the octahedral Δ value of Ni^{2+}-doped MgO (8650 cm^{-1})[24] or—multiplied by $^4/_9$—the typical values for the ligand field parameters of Co^{2+} and Ni^{2+} in tetrahedral oxygen coordination[24] ($\Delta_t \simeq 4000$ cm^{-1}). The electronic energy gain due to the lowering of the $^3B_{2g}$ ground state with respect to the tetrahedral $^3_aT_1$ ground state (hole formalism) is calculated to be 2600 cm^{-1}. The corresponding ground-state stabilization for Li_2CuO_4 is by far larger (9900 cm^{-1}) and would still amount to 6700 cm^{-1}, if the AO parameters of Li_2NiO_2 are used. Apparently the square-planar ligand geometry is imposed on Ni^{2+} by the specific packing conditions in the Li_2MO_2 ($M = Cu^{2+}$, Ni^{2+}) structure, obviously without a significant vibronic energy stabilization with respect to a tetrahedral "NiO_4" entity. The $^3B_{2g}$ ground state originates from the excited tetrahedral $e^3t_2^5(^3T_2)$ configuration, while usually square-planar Ni^{2+} induces a diamagnetic $^1_aA_{1g}$ ground state (from $e^2t_2^6$ in T_d, see Figure 6). This state is calculated here to occur at 6300 cm^{-1} above $^3B_{2g}$, though it is observed as the ground state even with oxygen as ligator atoms in some complexes. With the (larger) AO parameters of Li_2CuO_2 a diamagnetic $^1_aA_{1g}$ ground state would result also in this case, which lies only 200 cm^{-1} below the first triplet term $^3_aE_g$ ($^3_aT_1$), however. The electronic stabilization energy with respect to the tetrahedral $^3_aT_1$ ground state is reduced from 2600 to 2100 cm^{-1}. These findings indeed hint toward anomalous bonding properties. We think that the square-planar NiO_4 coordination is mainly stabilized by the specific packing and cooperative-elastic forces (strain contribution, accounted for by S_e) of the Li_2CuO_2 structure type. This argument is supported by the results of the next section. In agreement with the paramagnetism of Li_2NiO_2 a broad and apparently exchange-averaged EPR signal at $g \simeq 2.21_5$ is observed.

D. Ni^{2+} Tetrahedra in Spinel Phases. Unfortunately it is not possible to extract reliable AO parameters for the NiO_4 polyhedra in spinel mixed crystals $Zn_{1-x}Ni_xCr_2O_4$ from the ligand field spectra (Figure 8). Having in mind that the electronic stabilization energy of the NiO_4 square planes in Li_2NiO_2 with respect to the tetrahedral entity is comparatively small, we may choose the AO parameters for Li_2NiO_2 here as well. With these parameters the first- and second-order vibronic constants were calculated from (1.1) and (1.4) as $V_e = 4150$ cm^{-1} $Å^{-1}$ and $L_e = 1350$ cm^{-1} $Å^{-2}$ and from (1.5) and (1.6) as $V_e' \simeq 1250$ cm^{-1} $Å^{-1}$ and $L_e' \simeq 250$ cm^{-1} $Å^{-2}$ (Table I). If K_e is chosen as for Cu^{2+} (which is surely a reasonable assumption), ζ is fixed at $\simeq 0.70\zeta_0$, and the Racah parameter B has a value of 850 cm^{-1}, the cross sections of the potential energy surfaces shown in Figure 7a result, which arise from the $^3T_1$ ground-state manifold along the Q_θ coordinate. Obviously the system remains undistorted, though the Γ_1 potential curve is slightly asymmetric and rather broad, indicating a softening of the e mode. For smaller ζ parameters (for example due to a Ham effect[15]) a D_{2d} distortion (elongation) is expected. It amounts to $\rho = 0.17$ Å for vanishing LS coupling, with a stabilization energy of 240 cm^{-1} with respect to T_d symmetry.

It is already obvious at this stage of the discussion that Cu^{2+} undergoes a considerably larger Jahn–Teller coupling than Ni^{2+}. Apparently the main reason is that—due to the $^3_aT_1 - {}^3_bT_1$ configuration interaction—V_e^{eff} ($\simeq 2900$ cm^{-1} $Å^{-1}$, eq 5) and L_e^{eff} parameters ($\simeq 1050$ cm^{-1} $Å^{-2}$) have to be used instead of the considerably larger V_e and L_e coupling constants. The term mixing coefficient a, defined by (6), is 0.93_5. Because the signs of L_e are different for the two metal ions (eq 1.4), a further reduction of the vibronic stabilization is expected (eq 7).

Again following Woitowicz,[14] we have derived $S_e \cdot \rho \simeq 370$ cm^{-1} for the cooperative elastic energy in $NiCr_2O_4$ from the transition temperature ($T_c = 298$ K). With $\rho = 0.24$ Å ($2\theta = 102.5°$) one obtains $S_e = 1540$ cm^{-1} $Å^{-1}$. The inclusion of S_e into the vibronic calculation (with the parameters of Figure 7a) yields a ground-state potential energy surface that possesses only one rather broad minimum along $\varphi = 0$. The radial distortion parameter is $\rho = 0.24$ Å, which matches perfectly with the experimental value. As depicted in Figure 7b, the stabilization energy with respect to the T_d symmetry is 190 cm^{-1}. This result implies that the observed distortion of the NiO_4 tetrahedra in $NiCr_2O_4$ arises exclusively from cooperative elastic forces. Though the local Jahn–Teller coupling does not energetically stabilize the ground state (Figure 7a), it determines the sign of the cooperative unit cell distortion toward $c/a > 1$, because the potential energy curve is less steep for $\varphi = 0°$ than for $\varphi = 180°$.

The given interpretation is in accord with the ligand field spectra of the mixed crystals $Zn_{1-x}Ni_xCr_2O_4$ (Figure 8). They arise from Ni^{2+} and Cr^{3+} color centers, which occupy the tetrahedral and

(23) Reinen, D. *Theoret. Chim. Acta* **1966**, *5*, 312.
(24) Reinen, D. *Ber. Bunsen-Ges. Phys. Chem.* **1965**, *69*, 82.

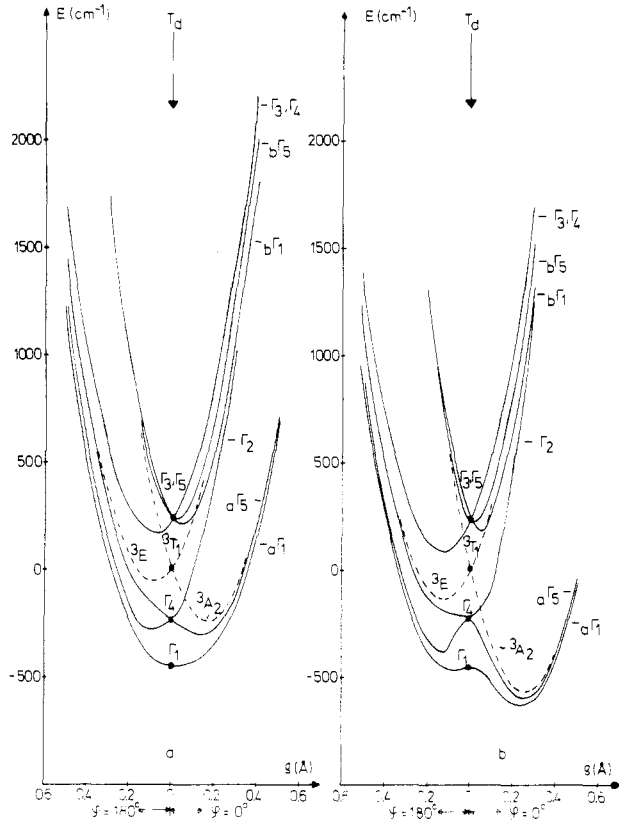

Figure 7. Cross sections of the potential energy surfaces, arising from the $^3_aT_1$ ground state of tetrahedral Ni^{2+}: (a) along the Q_θ coordinates (φ = 0 and 180°, 120 and 300°, or 240 and 60°), (b) along the Q_θ coordinate (φ = 0 and 180°), but with the inclusion of cooperativity (S_e = 1550 cm^{-1} $Å^{-1}$). Parameters: e_σ = 4700 cm^{-1}, e_π = 1300 cm^{-1}, $e_{d\delta}$ = 500 cm^{-1}, ζ = −450 cm^{-1}, and K_e^* = 17 500 cm^{-1} $Å^{-2}$. Solid and dashed curves correspond to energies with and without LS coupling.

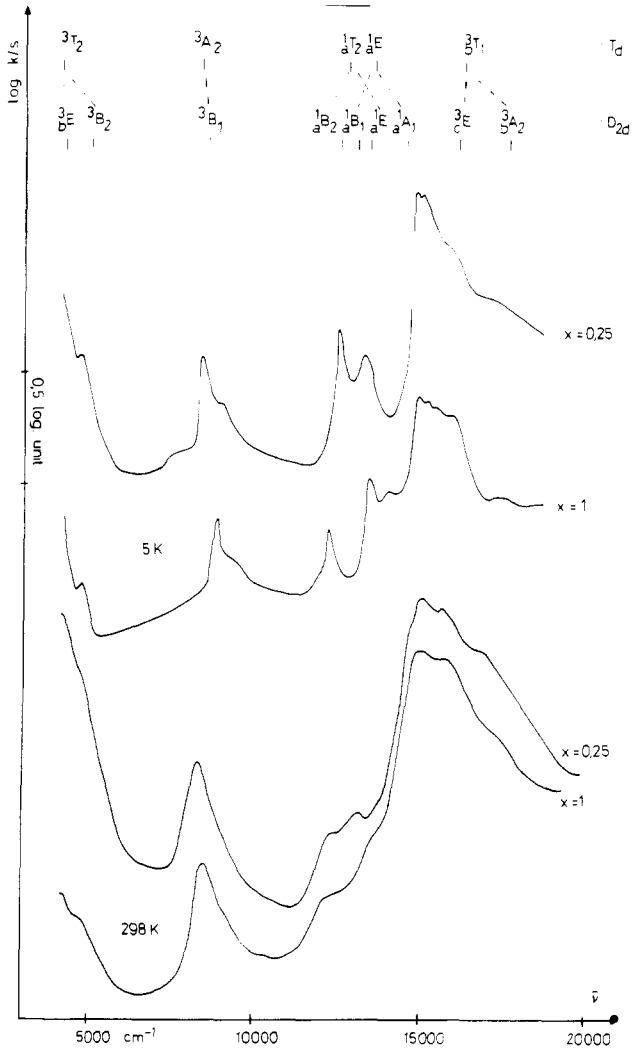

Figure 8. Electronic reflection spectra of mixed crystals $Zn_{1-x}Ni_xCr_2O_4$ at 298 and 5 K. Fitting parameters for tetrahedral Ni^{2+}: e_σ = 4700 cm^{-1}, e_π = 1200 cm^{-1}, B = 850 cm^{-1}, C/B = 4.0, ζ = −450 cm^{-1}, 2θ = 109.5° (x = 0.25) or 102.5° (x = 1.0). Only the average energies over the LS-split components are given; the ^3_aE ($^3_aT_1$) term is calculated at 1350 cm^{-1}.

octahedral sites of the spinel lattice, respectively. As is known from the spectrum of $ZnCr_2O_4$[25] the absorption around 17 200 cm^{-1} and the two sharp peaks in the region of 15 000 cm^{-1} have to be assigned to the $^4A_{2g} \rightarrow {}^4T_{2g}$ and $^4A_{2g} \rightarrow {}^2_aE_g$, $^2_aT_{1g}$ transitions of Cr^{3+}, respectively. We have fitted the spectra in T_d (x = 0.25) and D_{2d} symmetry (x = 1.0) by diagonalizing the complete d^8 matrices within the AO model, with the inclusion of LS coupling and the tetrahedral angles suggested for x = 0.25 (109.5°) and observed for x = 1.0 (102.5°). In case of $NiCr_2O_4$ the decrease of the $^3_aA_2$ ground state by the cooperativity ($S_e \cdot \rho \approx 350$ cm^{-1}) has been additionally taken into account. In Figure 8 only the average energies over the LS-split components are given. The narrow bands between 12 000 and 14 500 cm^{-1}, due to triplet–singlet transitions, are different in energy and number for x = 1 and x values below the critical concentration of the phase transition from tetragonal to cubic and can well be accounted for by the assumption of D_{2d} and T_d symmetries, respectively. From the triplet–triplet bands, only the transition around 9000 cm^{-1} shifts significantly to higher energies on going from x = 0.25 to 1.0. At 5 K in particular the spin-forbidden bands are much better resolved and have distinctly larger intensities. Ni^{2+} – Cr^{3+} interactions may strongly influence the intensities of those transitions and are presumably also responsible for the satellite in the band around 9000 cm^{-1}, which cannot be explained otherwise.

In contrast to the situation for Cu^{2+}, the transition energies in the ligand field spectra of Figure 8 can be fitted by using widely differing sets of e_σ and e_π parameters, as long as they obey

$$\Delta_t = \frac{4}{9}(3e_\sigma - 4e_\pi) \simeq 4100 \text{ cm}^{-1}$$

Thus AOM parameters extracted from the spectra of lower symmetry Ni^{2+} complexes, which are reported in the literature, should be viewed with caution. We have adjusted the e_σ and e_π parameters used with respect to those of Li_2NiO_2 and by comparison with the parameters of the isostructural Cu^{2+} compounds—as was outlined above.

Topology of the T ⊗ (e + t_2) Potential Energy Surface for Tetrahedral Cu^{2+} and Ni^{2+}. Now that bonding parameters and bending mode force constants for tetrahedral Cu^{2+} and Ni^{2+} complexes are available (Table II) they can be used in a comparative study of the Jahn–Teller stabilization energies E_{JT} (eq 7), which characterize the minima of the adiabatic potential energy surface. The maximal (epikernel) symmetry of the T ⊗ (e + t_2) interaction was found to be C_{2v}, whereas for the separate T ⊗ e problem it is D_{2d}. The maximal epikernel symmetries of the T ⊗ t_2 coupling are C_{3v} and C_{2v}, though it was shown that the absolute minima have C_{3v} symmetry.[7] Table II lists the Jahn–Teller stabilization energies for tetrahedral CuX_4^{2-} and NiO_4^{2-} chromophores, without considering spin–orbit coupling but with second-order vibronic terms accounted for. It can be readily seen that the D_{2d} extremal points (absolute minima in the T ⊗ e potential surface) are lowest in energy for all Cu^{2+} and Ni^{2+} chromophores, while the absolute minima for the full T ⊗ (e + t_2) problem (C_{2v} symmetry) are more stable than the C_{3v} minima of the T ⊗ t_2 potential surface. In agreement with the available structural data, the Cu^{2+} ion in a tetrahedral environment indeed

(25) Reinen, D. *Struct. Bonding (Berlin)* **1969**, *7*, 114.
(26) Nakamoto, K. *Infrared and Raman Spectra of Inorganic and Coordination Compounds*, 3rd ed.; Wiley: New York, 1978.

Table II. Jahn–Teller Stabilization Energies (cm^{-1}), Corresponding to Stationary Points of the Adiabatic T ⊗ (e + t_2) [C_{2v}], T ⊗ e [D_{2d}], and T ⊗ t_2 [C_{3v}] Potential Energy Surfaces of Cu^{2+} and Ni^{2+} in Tetrahedral Coordination (without Spin–Orbit Coupling)[a]

	first-order JT interaction			first- and second-order JT interaction		
complex	$E_{JT}(D_{2d})$	$E_{JT}(C_{3v})$	$E_{JT}(C_{2v})$	$E_{JT}(D_{2d})$	$E_{JT}(C_{3v})$	$(E_{JT}(C_{2v})$
$CuCl_4^{2-}$	−1630	−120	−495	−2250	−175	−395
$CuBr_4^{2-}$	−1320	−170	−460	−1545	−200	−300
CuO_4^{6-} [b]	−635	−35	−185	−700	−40	−165
	(−560)	(−25)	(−160)	(−610)	(−30)	(−140)
NiO_4^{6-} [b,c]	−530	−30	−150	−490	−25	−175
NiO_4^{6-} [b,d]	−260	−25	−80	−245	−20	−95
CuF_4^{2-}	−1325	−40	−360	−1560	−50	−310

[a] Parameter values used in the calculation ($K_t = K_e$): $CuCl_4^{2-}$, R = 2.23 Å, $e_{\sigma(\pi)}$ = 5690 (1390) cm^{-1},[24] K_e = 5700 cm^{-1} $Å^{-2}$ (from IR data);[26] $CuBr_4^{2-}$, R = 2.38 Å, $e_{\sigma(\pi)}$ = 4620 (820) cm^{-1},[24] K_e = 5000 cm^{-1} $Å^{-2}$ (value for $ZnBr_4^{2-}$);[26] CuF_4^{2-}, R = 2.08 Å, $e_{\sigma(\pi)}$ = 5850 (1850) cm^{-1}, K_e = 8500 cm^{-1} $Å^{-2}$ (estimate from IR data);[26] CuO_4^{6-}, R = 1.94 Å, $e_{\sigma(\pi)}$ = 5700 (2000) cm^{-1}, K_e = 16450 cm^{-1} $Å^{-2}$, with values in parentheses calculated with $e_{\sigma(\pi)}$ = 4900 (1400) cm^{-1} and e_{sd} = 1800 cm^{-1}; NiO_4^{6-}, R = 1.93 Å, $e_{\sigma(\pi)}$ = 4700 (1300) cm^{-1}, K_e = 16 450 cm^{-1} $Å^{-2}$. [b] Formal charges, because polyhedra are interconnected in the spinel structure (see text). [c] Without inclusion of configuration interaction between the two tetrahedral $^3T_2$ states. [d] With inclusion of configuration interaction between the two states.

interacts predominantly with the Q_θ component of the e mode. We expect that these rather strong interactions usually dominate over steric lattice and spin–orbit coupling effects.

In contrast Ni^{2+} in tetrahedral complexes suffers moderate to weak Jahn–Teller coupling. As was previously discussed above, configuration interaction markedly depresses the vibronic coupling parameters and the Jahn–Teller stabilization energy $|E_{JT}|$ along the D_{2d} distortion pathway in this case (Table II). $|E_{JT}|$ depends on the square of V_e (V_e^{eff}) and thus diminishes even faster than the vibronic constant itself (see (7)). The effective vibronic constant V_t^{eff} for the T ⊗ t_2 problem is obtained in a manner similar to that used for V_e^{eff}:

$$V_t^{eff} = \left(a^2 + \frac{1}{2}b^2\right)V_t \qquad (11)$$

with a and b as defined in (6). It is easily seen by comparing (5) and (11) that the inclusion of configuration interaction has a much stronger influence on $E_{JT}(e)$ than on $E_{JT}(t_2)$. A reduction of $|E_{JT}|$ is also calculated for the C_{2v} minima. Accounting for spin–orbit coupling will further reduce $|E_{JT}|$ as was shown above for the T ⊗ e interaction (Figure 7a). One may conclude for NiX_4 chromophores that, in ligand fields of moderate strength, the Jahn–Teller stabilization is small in all minima. We expect that rigid lattice, steric ligand, or spin–orbit effects can be comparable in magnitude to the vibronic Jahn–Teller coupling. The interplay between these various interactions may thus lead to D_{2d}, C_{2v}, C_{3v} or even lower symmetry distortions, depending on the relative magnitudes of the mentioned electronic and elastic perturbations. Cooperative elastic interactions between the tetrahedra, which may be strong in structures with interconnected polyhedra, frequently enhance the ground-state splitting and the extent of the local Jahn–Teller distortions, leading to lower symmetry unit cells.

Summary and Concluding Remarks

Introducing a vibronic coupling model that includes both configuration interaction and spin–orbit coupling, we have shown that the extent of the Jahn–Teller distortion in the tetrahedral $^3T_1$ and $^2T_2$ ground states of Ni^{2+} and Cu^{2+}, respectively, should be distinctly larger in the latter case—in agreement with the available experimental data. If we refer to eq 1, 5, and 7 and Table I, it is immediately evident, that the reduction of ρ_m on going from Cu^{2+} to Ni^{2+} is mainly due to the linear vibronic coupling. The configuration interaction between the two $^3T_1$ terms induces a reduction of the linear vibronic coupling constant by about 30%. ρ_m for Ni^{2+} will be further reduced with respect to Cu^{2+}, if the second-order coupling parameter L_e is taken into account and K_e is considered to be equal for both cations (eq 7). The latter effect corresponds to an increase of K_{eff}^* by more than 15%.

It is expected that ligands with greater e_σ and smaller e_π as well as B parameters may induce considerably larger V_e^{eff} constants, because not only V_e will increase but also the configuration interaction between the two $^3T_1$ terms should become smaller. This is supported by experiment. While the $NiCl_4^{2-}$ tetrahedra in $[AsPh_3CH_3]_2NiCl_4$[27] are undistorted within the error limit, the NiN_4 chromophores in $Cat[Ni(NCS)_4]$[3] (Cat = *p*-xylylenebis(triphenylphosphonium)$^{2+}$) exhibit rather large static distortion components due to vibronic Jahn–Teller forces. Unfortunately 4-coordinate Ni^{2+} will adopt a square-planar geometry and a singlet ground state, if ligands with even larger Δ/B ratios are present. Thus, the range of Δ/B values that could prove our concept is rather limited. If large deviations from the ideal tetrahedral angle are observed, the energetic influence of ligand–ligand repulsions, which are not included in our model, cannot be disregarded anymore. Such repulsions will destabilize the elongated tetrahedra more than the compressed ones.

Interestingly enough, Ni^{2+} can also be stabilized in a linear coordination of two oxygen ligator atoms (K_2NiO_2; a(Ni–O) = 1.68 Å).[28] We observe two absorption bands at ≃8500 and ≈1500 cm^{-1} (298 K) in the reflection spectrum and a broad, apparently exchange-averaged EPR signal (298 K) at $g \simeq 2.19_5$, in accord with the reported[28] high-spin behavior of K_2NiO_2. The orbitally doubly degenerate $^3\pi_g$ groundstate (point group $D_{\infty h}$) originates from (z^2; xz, yz) (hole formalism) and is stable with respect to further distortion (Renner effect). A single-crystal study of the electronic spectrum is forthcoming.[29]

If the Jahn–Teller distorted polyhedra are involved in strong cooperative elastic interactions within the host lattice, large contributions to the observed term splittings may arise from electronic effects induced by cooperative–elastic forces. Thus, the observed static distortion of the NiO_4 tetrahedra in spinel mixed crystals $Zn_{1-x}Ni_xCr_2O_4$ at very high x values is apparently induced by the action of the cooperative Jahn–Teller effect. Without cooperativity and depending on the magnitude of ζ, the system either remains in T_d symmetry (with a softening of the e mode) or induces only small ρ_m values, which may lead to a dynamic Jahn–Teller effect even at room temperature.

It is also of interest to study the influence of rigid ligand or crystal packing effects within a host structure on the potential surfaces of Jahn–Teller ions, because observed deviations from the ideal T_d symmetry are frequently at least partly of nonelectronic origin. The comparison of the Cu^{2+} and Ni^{2+} compounds with the analogous Zn^{2+} or Co^{2+} compounds is usually helpful, because the latter complexes have orbitally nondegenerate ground states in tetrahedral ligand fields and are not subject to Jahn–Teller forces. Thus the structures of compounds $Cat[M(NCS)_4]$ (M = Co^{2+}, Ni^{2+}, Cu^{2+})[3] reveal that packing forces already induce a tetragonal compression of the "MN_4" tetrahedra (for Co^{2+}, 2θ = 115°). This compression is consideraly enhanced in case of Cu^{2+} (2θ = 137°), due to the Jahn–Teller interaction of "the same sign". In case of Ni^{2+} the Jahn–Teller forces act in a direction

(27) Pauling, P. *Inorg. Chem.* **1966**, *5*, 1498.
(28) Rieck, H.; Hoppe, R. *Z. Anorg. Allg. Chem.* **1973**, *400*, 311.
(29) Hitchman, M. A.; Stratemeier, H.; Hoppe, R., manuscript in preparation.

opposite to the packing effect and stabilize (approximately) a geometry with C_{2v} symmetry (2θ = 115.5, 126.5°). Similarly interesting are the orthorhombic phases observed for spinel mixed crystals $Ni_xCu_{1-x}Cr_2O_4$ with $0.860 \geq x \geq 0.825$.[3] The static D_2 distortion of the NiO_4 and CuO_4 tetrahedra in this concentration range is the result of the combined action of Jahn–Teller couplings and the symmetry lowering due to cooperative elastic interactions between the transition-metal polyhedra. The latter ($NiCr_2O_4$, $c/a > 1$; $CuCr_2O_4$, $c/a < 1$) are always opposite in the sign of distortion to those induced by the electronic effects of Cu^{2+} (compression) and Ni^{2+} (elongation), incorporated into $NiCr_2O_4$ and $CuCr_2O_4$, respectively. The influence of a lattice strain with the same sign of distortion as the Jahn–Teller coupling on the potential surface was discussed above (Figure 7b). A group-theoretical analysis of the described phenomena for MN_4 and MO_4 chromophores (M = Cu^{2+}, Ni^{2+}) is given elsewhere.[3]

Acknowledgment. M.A. is grateful to the University of Marburg and the German Science Foundation (DFG) for providing financial help during his stay in the FRG. Partial financial support by the Council of Science, Bulgaria, is also acknowledged. We owe thanks to Dr. B. Jakob (Marburg) for experimental contributions and Dr. M. A. Hitchman (Hobart) for extensive discussions.

Appendix

The vibronic Hamiltonian of the $T \otimes (e + t_2)$ problem including linear and quadratic terms was given previously.[7] (Some misprints in eq 10 of ref 7 are as follows: second row, the term $^1/_2Q_\zeta^2$ should read $^1/_4Q_\zeta^2$; fourth (fifth) row, a minus sign in front of $^1/_2Q_\theta Q_\xi$ ($^1/_2Q_\theta Q_\eta$) should be added; sixth row, the term $X_\zeta Q_\zeta Q_\eta$ should read $X_\zeta Q_\xi Q_\eta$.) The part relevant for our discussion ($T \otimes e$ problem) is

$$\mathbf{H} = \frac{1}{2}K_e(Q_\theta^2 + Q_\epsilon^2)\mathbf{I} + \left[V_eQ_\theta + L_e\left(\frac{1}{2}Q_\epsilon^2 - \frac{1}{2}Q_\theta^2\right)\right]\mathbf{C}_\theta + [V_eQ_\epsilon + L_eQ_\theta Q_\epsilon]\mathbf{C}_\epsilon$$

where $\mathbf{I}$ is the unit matrix, and

$$\mathbf{C}_\theta = \begin{pmatrix} 1/2 & 0 & 0 \\ 0 & 1/2 & 0 \\ 0 & 0 & -1 \end{pmatrix}$$

$$\mathbf{C}_\epsilon = \begin{pmatrix} -3^{1/2}/2 & 0 & 0 \\ 0 & 3^{1/2}/2 & 0 \\ 0 & 0 & 0 \end{pmatrix}$$

The labeling order of rows and columns corresponds to $T_1\alpha$, $T_1\beta$, and $T_1\gamma$ for the T_1 state (d^8) and $T_2\xi$, $T_2\eta$, and $T_2\zeta$ for the T_2 state (d^9); K_e is the e mode force constant

$$K_e = \frac{1}{2}\left\langle T\left|\left(\frac{d^2V}{dQ_\theta^2} + \frac{d^2V}{dQ_\epsilon^2}\right)_0\right|T\right\rangle$$

and the first and second order JT coupling constants V_e and L_e are defined as

$$V_e = -\left\langle T_1\gamma\left|\left(\frac{dV}{dQ_\theta}\right)_0\right|T_1\gamma\right\rangle = -\left\langle T_2\zeta\left|\left(\frac{dV}{dQ_\theta}\right)_0\right|T_2\zeta\right\rangle$$

$$L_e = \frac{1}{2}\left\langle T_1\gamma\left|\left(\frac{d^2V}{dQ_\theta^2} - \frac{d^2V}{dQ_\epsilon^2}\right)_0\right|T_1\gamma\right\rangle = \frac{1}{2}\left\langle T_2\zeta\left|\left(\frac{d^2V}{dQ_\theta^2} - \frac{d^2V}{dQ_\epsilon^2}\right)_0\right|T_2\zeta\right\rangle$$

We can simplify $\mathbf{H}$ by setting $Q_\theta = \rho\cos\varphi$ and $Q_\epsilon = \rho\sin\varphi$ and obtain the diagonal form of $\mathbf{H}$ with matrix elements:

$$\langle T_1\alpha|\mathbf{H}|T_1\alpha\rangle = \langle T_2\xi|\mathbf{H}|T_2\xi\rangle = \frac{1}{2}\left(K_e - \frac{1}{2}L_e\cos 2\varphi - \frac{3^{1/2}}{2}L_e\sin 2\varphi\right)\rho^2 + \frac{1}{2}V_e\rho(\cos\varphi - 3^{1/2}\sin\varphi)$$

$$\langle T_1\beta|\mathbf{H}|T_1\beta\rangle = \langle T_2\eta|\mathbf{H}|T_2\eta\rangle = \frac{1}{2}\left(K_e - \frac{1}{2}L_e\cos 2\varphi + \frac{3^{1/2}}{2}L_e\sin 2\varphi\right)\rho^2 + \frac{1}{2}V_e\rho(\cos\varphi + 3^{1/2}\sin\varphi)$$

$$\langle T_1\gamma|\mathbf{H}|T_1\gamma\rangle = \langle T_2\zeta|\mathbf{H}|T_2\zeta\rangle = \frac{1}{2}(K_e + L_e\cos 2\varphi)\rho^2 - V_e\rho\cos\varphi$$

Taking into account strains due to cooperative elastic forces, an additional term $\mathbf{H}_s$ is introduced, which reflects the external force, transmitted by the lattice to the JT center via the localized e mode[13]

$$\mathbf{H}_s = S_\theta Q_\theta^s + S_\epsilon Q_\epsilon^s$$

where S_θ and S_ϵ are defined as the strain forces for a distortion, whose magnitude equals the zero point displacement amplitude of the θ or ϵ component of the e mode. $\mathbf{H}_s$ has the symmetry of the linear coupling terms in $\mathbf{H}$, and one obtains for strains of D_{2d} symmetry

$$\mathbf{H}_s = +(-)S_e\rho\mathbf{C}_\theta$$

[compression (elongation) along the S_4 axis; $S_e \lesssim 0$ for d^9 and d^8, respectively].

The corresponding strain energy should be added to the linear coupling terms in the energy matrix. Accounting also for the spin–orbit coupling, the following off-diagonal matrix elements for the $^3T_1$ and $^2T_2$ manifolds (first-order LS coupling) result:

$^3T_1$

$$\frac{i}{2^{1/2}}\langle {}^3T_1\alpha \pm 1|\mathbf{H}_{LS}|{}^3T_1\beta \pm 1\rangle = \langle {}^3T_1\alpha \pm 1|\mathbf{H}_{LS}|{}^3T_1\gamma 0\rangle = \langle {}^3T_1\alpha 0|\mathbf{H}_{LS}|{}^3T_1\gamma \mp 1\rangle = \mp\zeta/2(2^{1/2})$$

$$-i\langle {}^3T_1\beta \pm 1|\mathbf{H}_{LS}|{}^3T_1\gamma 0\rangle = -i\langle {}^3T_1\beta 0|\mathbf{H}_{LS}|{}^3T_1\gamma \pm 1\rangle = \zeta/2(2^{1/2})$$

$^2T_2$

$$-i\left\langle {}^2T_2\xi\frac{1}{2}|\mathbf{H}_{LS}|{}^2T_2\eta\frac{1}{2}\right\rangle = -\left\langle {}^2T_2\xi\frac{1}{2}|\mathbf{H}_{LS}|{}^2T_2\zeta - \frac{1}{2}\right\rangle = -i\left\langle {}^2T_2\eta\frac{1}{2}|\mathbf{H}_{LS}|{}^2T_2\zeta - \frac{1}{2}\right\rangle = \zeta/2$$

The vibronic coupling constants V_e' and L_e', which are used to define the effective parameters V_e^{eff} and L_e^{eff} for a $^3T_1$ ground state (eq 5), are denoted as follows:

$$V_e' = \left\langle \epsilon\left|\frac{dV}{dQ_\theta}\right|\epsilon\right\rangle$$

$$L_e' = \left\langle \epsilon\left|\frac{d^2V}{dQ_\epsilon^2}\right|\epsilon\right\rangle = -\left\langle \epsilon\left|\frac{d^2V}{dQ_\theta^2}\right|\epsilon\right\rangle$$

The linear vibronic constants for the t_2 bending and stretching modes (eq 1.2 and 1.3) are defined by ($^2T_2$ ground state)

$$V_t^b = -\left\langle {}^2T_2\xi\left|\frac{dV}{dQ_\zeta^b}\right|{}^2T_2\eta\right\rangle$$

$$V_t^s = -\left\langle {}^2T_2\xi\left|\frac{dV}{dQ_\zeta^s}\right|{}^2T_2\eta\right\rangle$$

Registry No. $CuCl_4^{2-}$, 15489-36-8; $CuBr_4^{2-}$, 14337-09-8; CuO_4^{6-}, 56509-86-5; NiO_4^{6-}, 113857-72-0; CuF_4^{2-}, 67415-38-7; Ni^{2+}, 14701-22-5; Cu^{2+}, 15158-11-9; $Zn_{1-x}Cu_xCr_2O_4$, 113924-15-5; $Zn_{1-x}Ni_xCr_2O_4$, 113924-16-6.